THERMODYNAMIC LOSSES IN A GAS SPRING: COMPARISON OF EXPERIMENTAL AND NUMERICAL RESULTS

Sapin P.[1,*], Taleb A.[1], Barfuss C.[1], White A.J.[2], Fabris D.[1,3] and Markides C.N.[1]

[*]Author for correspondence
E-mail: p.sapin@imperial.ac.uk

[1]Clean Energy Processes (CEP) Laboratory,
Department of Chemical Engineering,
Imperial College London,
London, United Kingdom

[2]Department of Engineering,
University of Cambridge,
Cambridge,
United Kingdom

[3]Department of Mechanical Engineering,
Santa Clara University,
Santa Clara, California
USA

ABSTRACT

Reciprocating-piston devices can be used as high-efficiency compressors and/or expanders. With an optimal valve design and by carefully adjusting valve timing, pressure losses during intake and exhaust can be largely reduced. The main loss mechanism in reciprocating devices is then the thermal irreversibility due to the unsteady heat transfer between the compressed/expanded gas and the surrounding cylinder walls. In this paper, pressure, volume and temperature measurements in a piston-cylinder crankshaft driven gas spring are compared to numerical results. The experimental apparatus experiences mass leakage while the CFD code predicts heat transfer in an ideal closed gas spring. Comparison of experimental and numerical results allows one to better understand the loss mechanisms in play. Heat and mass losses in the experiment are decoupled and the system losses are calculated over a range of frequencies. As expected, compression and expansion approach adiabatic processes for higher frequencies, resulting in higher efficiency. The objective of this study is to observe and explain the discrepancies obtained between the computational and experimental results and to propose further steps to improve the analysis of the loss mechanisms.

INTRODUCTION

Clean energy production from renewable sources such as solar or wind power faces major technological challenges. Effective use of such intermittent sources requires the development of large-scale energy storage technologies such as Pumped Thermal Electricity Storage (PTES), a system based on a reversible Joule-Brayton cycle, and the improvement of low-temperature energy conversion systems, including organic Rankine cycles. The performance of these thermodynamic cycles is adversely affected by different sources of irreversibility, in particular by the losses associated with the compression and expansion processes. Reciprocating-piston compressors and expanders are being proposed because of their potentially higher efficiency at high compression ratios, in comparison with turbomachines at relative smaller-scale application.

NOMENCLATURE

BDC	[-]	Bottom Dead Center
c	[m/s]	Speed of sound
c_p	[J/kg.K]	Specific heat capacity at constant pressure
D	[m]	Bore diameter
D_h	[m]	Hydraulic diameter
h	[J/kg]	Specific enthalpy
L_dv	[m]	Dead volume height
L_r	[m]	Connecting rod length
L_s	[m]	Stroke length
m	[kg]	Mass
$\dot{m}$	[kg]	Mass flow rate
Nu	[-]	Nusselt number
P	[Pa]	Pressure
P_r	[-]	Pressure ratio
Pe_ω	[-]	Oscillatory Péclet number
$\dot{q}$	[W/m^2]	Wall heat flux
$\dot{Q}$	[W]	Wall heat flow rate
r	[m]	Radial coordinate
r_s	[m]	Crankshaft radius
R	[J/kg.K]	Specific gas constant
Re	[-]	Reynolds number
RPM	[-]	Revolution Per Minute
S_w	[m^2]	Total inner wall surface
t	[s]	Time
T	[K]	Gas temperature
T_l	[K]	Line-averaged temperature
T_m	[K]	Mass-averaged temperature
TDC	[-]	Top Dead Center
V	[m^3]	Volume
V_r	[-]	Volume ratio
z	[m]	Axial coordinate
z_p	[m]	Piston height relative to TDC

Greek characters

α	[m^2/s]	Thermal diffusivity
β	[rad]	Wedge angle (CFD geometry)
γ	[-]	Heat capacity ratio
θ	[rad]	Crank angle
Ψ	[-]	Non-dimensional cyclic loss
ω	[rad/s]	Rotational speed

Subscripts and superscripts

0	[rad]	Cycle average
a	[-]	Amplitude
CFD	[-]	Computational
th	[-]	Thermal
XP	[-]	Experimental

The unsteady heat exchange between the compressed-expanded gas and the cylinder walls of reciprocating devices has been studied both analytically and experimentally in gas

spring configurations, i.e. without complex effects of gas intake/exhaust. Pressure fluctuations within the compression chamber give rise to complex in-cylinder heat transfer, which affect not only their design and reliability but also their thermodynamic performance. In the early 40s, Pfriem [1] predicted a phase shift between the instantaneous heat flux at the wall and the bulk gas-to-wall temperature difference, which means that the classical Newton's law of cooling cannot be applied to characterize the gas-to-wall heat transfer. In 1983, Lee [2] introduced a model based on a complex Nusselt number, Nu, to account for this phase shift, valid only for low oscillating frequencies. Kornhauser and Smith [3,4] conducted experiments in reciprocating gas springs and provided Nu-Re correlations to predict the in-cylinder heat transfer. However, these correlations are restricted to low compression ratios and do not consider cyclic mass leakage because of the design of their experiment.

In the present work, experimental data are obtained on a crankshaft driven gas spring that experiences mass leakage through the clearance between piston and cylinder. Pressure, volume and temperature are measured over several cycles.

In addition, the heat transfer between the gas and the surrounding walls is modelled with a laminar CFD code solved with OpenFOAM for an ideal gas spring, i.e. without mass leakage. The comparison of experimental and CFD results allows one to better understand the overall system losses and more importantly to extract the leakage losses and estimate the contribution of thermal losses.

The main purpose of this project is to validate the CFD model with high-fidelity experimental data. With this aim in mind, this study presents a comparison of experimental and numerical data. The objective is to explain the discrepancies observed between the two approaches and to propose further steps to improve the analysis of the loss mechanisms in reciprocating gas springs.

EXPERIMENTAL METHODS

Experimental setup

The experimental setup is a crankshaft-driven piston-cylinder compressor operated as a gas spring with nitrogen. The valve system has been removed and replaced with a cylinder head equipped with measurement devices, as indicated in Figure 1. The dimensions of the system are:

Bore diameter $D = 105$ mm;
Stroke length $L_\mathrm{s} = 2 \cdot r_\mathrm{s} = 78$ mm;
Connecting rod length $L_\mathrm{r} = 148.5$ mm;
Dead volume height $L_\mathrm{dv} = 14$ mm;

The crankshaft is driven by an induction motor and the reciprocating motion of the piston is related to the crank angle, θ, according to the following relation:

$$z_\mathrm{p} = r_\mathrm{s}\,(1 - \cos\theta) + L_\mathrm{r}\left(1 - \sqrt{1 - \left(\frac{r_\mathrm{s}}{L_\mathrm{r}}\right)^2 \sin^2\theta}\right) \quad , \tag{1}$$

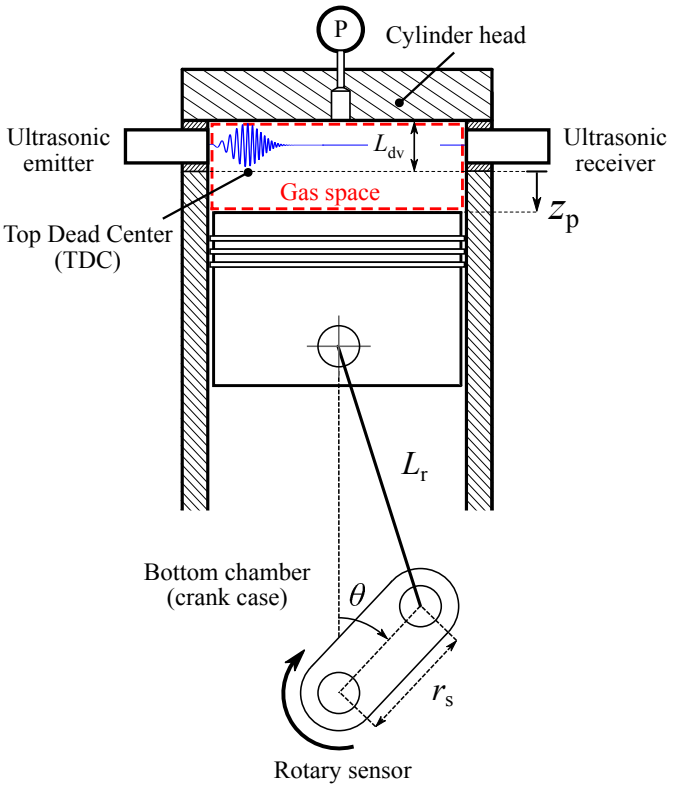

Figure 1. Sketch of the experimental setup.

where z_p is the distance between the piston head and top dead center (TDC) position, at which $\theta = 0$ (see Figure 1). The volume ratio of the system is variable but has been set to a value of $V_\mathrm{r} = 6.6$ in this study.

Mass leakage between the gas space and the crank case (maintained at atmospheric pressure) are limited through two piston rings seated in grooves on the outer diameter of the piston. The gas spring system experiences both mass and thermal losses. To decouple losses due to unsteady heat transfer from losses due to mass leakage, three bulk parameters are measured.

The pressure, P, is measured with a pressure transducer (PX35D0 by Omega – 0.25% accuracy) connected to the compression chamber through the cylinder head. A rotary sensor (shat encoder BMSV30 by BAUMER, 1024 steps per revolution) is used to measure the crank angle θ. The volume of the gas, V, is then calculated based on Equation (1).

The line-averaged gas temperature, T_l, is measured with a fast and non-invasive system using piezoelectric ceramic transducers to measure the speed of sound, c, in the gas space. A frequency modulated – or chirp – signal is emitted by an ultrasonic transducer and travels up to the diametrically opposed transducer, denoted as ultrasonic receiver in Figure 1. Cross-correlation of the emitted and received signals allows the time-of-flight of the pulse signal across the compression chamber to be calculated. This pulse compression method is described in detail by Mathie *et al.* [5]. Finally, the gas temperature is calculated with the relationship between T_l and c, that is,

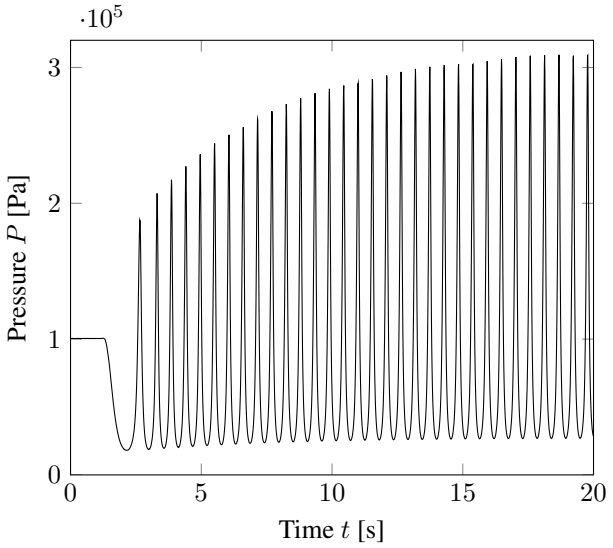

Figure 2. Pressure evolution during the first 20 seconds (over 80 seconds in total) of a run. Crank rotational speed $\omega = 109.34$ RPM.

for an isentropic wave propagation:

$$c = \sqrt{\gamma R T_\mathrm{l}} \quad , \tag{2}$$

where R and γ are respectively the specific gas constant and the heat capacity ratio (for nitrogen, $R = 298.14$ J/kg.K and $\gamma = 1.401$ at 300 K, according to Ref. [6]). The system effectively measures the average temperature along the distance separating the sensors, denoted T_l, that will be further used as an estimate of the bulk gas temperature, T.

Procedure and data acquisition

At the start of the run, the piston is placed at top dead center (TDC, $\theta = 0$ degrees). The motor is then started and P, V and T_l are recorded for 80 seconds. The pressure evolution is plotted in Figure 2 during the first 20 seconds. The mean pressure through the successive cycles increases with time up to reaching equilibrium approximately after 20 seconds. During the first oscillations, the mean pressure in the compression/expansion chamber is lower than atmospheric that prevails in the crank case. The mass leakage to and from the gas chamber result in a net increase of the mean mass in the system, and thus of the mean pressure.

In this article, experimental data only consider the last 20 cycles for each run, i.e. once equilibrium is reached, by which we mean that the cycle-to-cycle variation of the pressure at TDC is smaller than 0.5%. The data presented hereafter are averaged over these 20 cycles. Experiments are run for a range of motor frequencies, from 27 to 164 RPM (i.e. from 0.45 to 2.7 Hz).

At bottom dead center (BDC, $\theta = \pm 180$ degrees), temperature drops below 200 K. If humid air was used, ice crystals might nucleate, which could disturb the ultrasonic signal transmission. To remove humidity, the compression and the crank case are purged and filled with nitrogen before running the experiment.

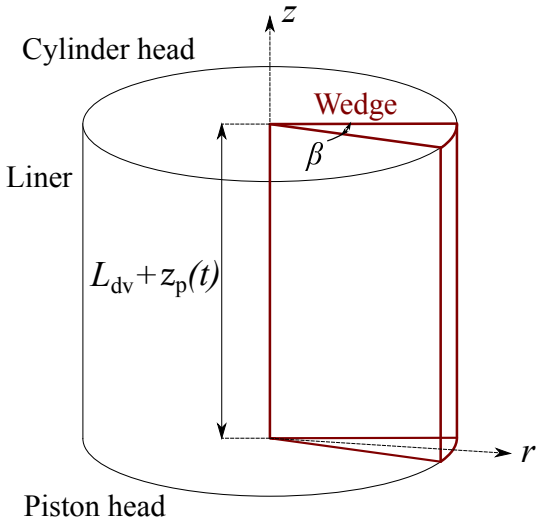

Figure 3. Modelled wedge geometry.

COMPUTATIONAL METHODS

A Computational Fluid Dynamics (CFD) model is built in the open source OpenFOAM code. The density, velocity, pressure and temperature fields are calculated in an ideal gas spring system (without mass leakage) by solving the ideal gas law and the mass, momentum and energy balance equations. The set of equations is solved with a modified version of the *coldEngineFOAM* solver using a PIMPLE algorithm, that is a combination of the SIMPLE (semi-implicit method for pressure linked equations) and PISO (pressure-implicit split operator) algorithms.

Geometry and mesh

Since the gas spring is axisymmetric, only a wedge is modelled. Figure 3 shows the geometry and the modelled wedge ($\beta = 0.02$ rad).

The cylinder head is the stationary upper boundary, while the lower boundary, i.e. the piston head, is a moving boundary whose motion is given by Equation (1). A quadrilateral dynamic mesh is used to model the changing volume of the compression space. The aspect ratio, i.e. the ratio between the radial and the axial mesh sizes, is chosen to be 1 at midstroke ($\theta = -90$ degrees during the upstroke and +90 during downstroke), away from the boundary layers where the mesh is refined. A convergence study has been carried out to investigate the independence of the results upon mesh resolution and Courant number. As expected, mesh resolution has to be increased for higher frequencies. For rotational speeds around 100 RPM, the optimal mesh resolution was found to be 90×90.

Initial and boundary conditions

Simulations are run for several cycles until the gas spring reaches cyclic steady state, starting from BDC ($\theta = -180$ degrees). The pressure at BDC is taken from the experimental measurement at equilibrium. The initial temperature is chosen such that the mass of nitrogen in the gas domain is the mean mass in the experiments.

However, the mass in the experimental gas spring, m, varies because of mass leakage and is estimated from the P, V and T_{l} measurements with the ideal gas equation of state:

$$m = \frac{PV}{RT} \approx \frac{PV}{RT_{\mathrm{l}}} \quad , \tag{3}$$

where T_{l} is the in-cylinder gas temperature measured with the ultrasonic transducers, which offers an estimate of the mass-averaged temperature, T_{m}, defined as:

$$T_{\mathrm{m}} = \frac{1}{m} \int \rho T \mathrm{d}V \quad . \tag{4}$$

This motivates the need to link T_{l} and T_{m} thanks to the temperature and density fields computed in the CFD model.

For the run at 109.34 RPM, the estimated mass varies between 2.96×10^{-4} and 3.48×10^{-4} kg, with a mean of 3.25×10^{-4} kg. The initial temperature imposed for this specific run in the computational model is thus 224.9 K.

As for boundary conditions, a no-slip condition is imposed for velocity and constant and uniform wall temperatures are applied. The choice of an isothermal wall boundary condition is supported by experimental results. Indeed, Adair *et al.* [7] carried out measurements in reciprocating compressors and observed that the cylinder wall temperature varies by less than 1 K. Lekic and Kok [8] have made similar assumptions to simulate Kornhauser and Smith's [3,4] experiments.

In prior work [9], the authors presented CFD results for a range of wall temperatures and its influence on P-V and T-V diagrams. A wall temperature of 290 K has shown a reasonable matching with experimental data. The cylinder head, piston head and liner wall temperatures are thus defined to be at constant temperature of 290 K for the present study.

RESULTS

In this section, experimental data are compared to the computational results. First, P-V (Pressure-Volume) and T-V (Temperature-Volume) diagrams are compared for a single run at 109.34 RPM. Then, the losses are calculated and compared over a range of frequencies.

Comparison of experimental and computational results for a single run at 109.34 RPM

Figure 4 shows a comparison of experimental and computational P-V diagrams. The experimental diagram is wider than the computational one, which means that the CFD underestimates the net work done on the gas over a cycle. In other words, the loss throughout one cycle is higher in the experiments than in the CFD. A rather important difference in the pressure reached at TDC is also observed, which results in a higher pressure ratio for the CFD. The experimental pressure ratio is only $P_{\mathrm{r}} = 11.76$, while it is 12.62 for the CFD. The numerical simulation is thus

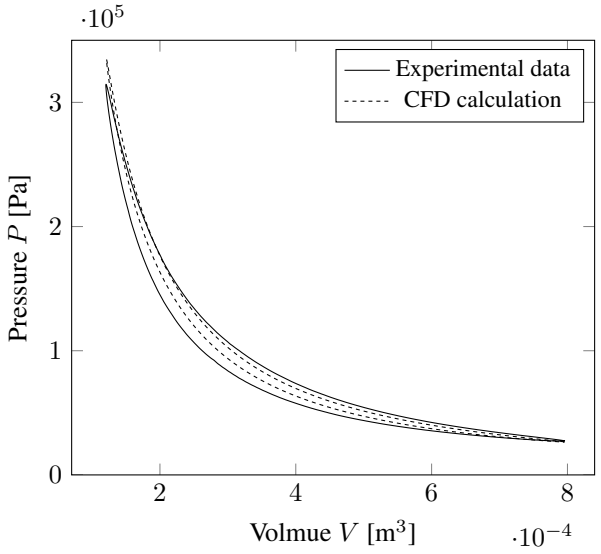

Figure 4. Experimental and computational P-V diagrams for a run at 109.34 RPM, mass of 3.25×10^{-4} kg and wall at 290 K.

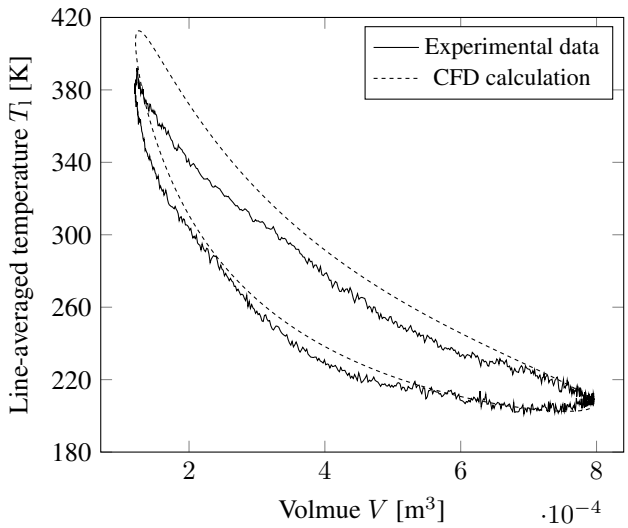

Figure 5. Experimental and computational T-V diagrams for a run at 109.34 RPM, mass of 3.25×10^{-4} kg and wall at 290 K.

closer to the adiabatic pressure ratio ($V_{\mathrm{r}}{}^{\gamma} = 14.04$), which also indicates a lower cycle loss. The observed discrepancy can be due to mass leakage, which is absent for the CFD simulation, whereas experimental losses include both thermal and mass losses. During compression, the pressure evolution is similar between computational and experimental results, while the highest difference is observed near TDC, when mass losses are expected to be largest.

Temperature measurements provide information about the specific thermodynamic state of the gas in the system. In Figure 5, the temperature evolution is compared relative to the instantaneous volume. For consistency, the temperature reported for the CFD calculation is a line-average of the radial temperature at the level of the ultrasonic transducers, i.e. 7 mm below

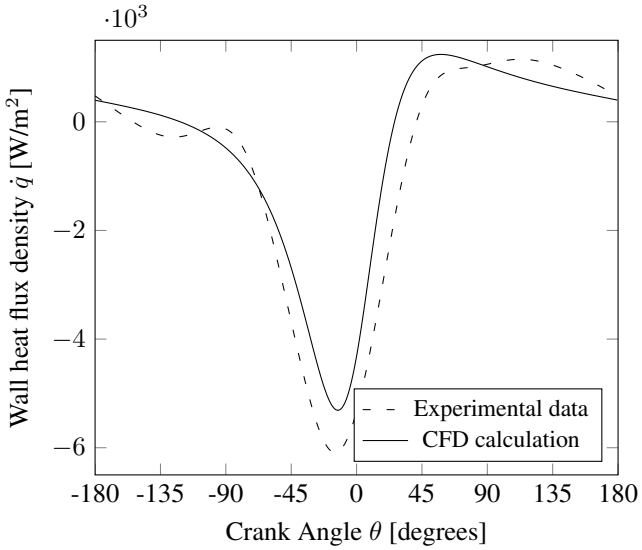

Figure 6. Experimental and computational wall heat flux density as a function of crank angle for a run at 109.34 RPM, mass of 3.25×10^{-4} kg and wall temperature of 290 K.

the cylinder head. Again, numerical calculation shows a good general agreement with the experimental data, though with a deviation at TDC of approximately 20 K. At small volume and high system pressure, the mass leakage induces a drop of the system enthalpy, resulting in a temperature drop.

To decouple losses due to heat transfer from losses induced by mass leakage in the experiments, the heat flux $\dot{Q}$ exchanged between the gas and the surrounding walls can be derived from the energy conservation equation for an open system. Indeed, the energy balance for the experimental gas spring takes the following form:

$$m\frac{\mathrm{d}h}{\mathrm{d}t} = \dot{Q} + V\frac{\mathrm{d}p}{\mathrm{d}t} + \dot{m}\,(h_{\mathrm{ex}} - h) \quad , \tag{5}$$

where h denotes the specific gas enthalpy, $\dot{m}$ is the leakage mass flow rate, and h_{ex} is the specific enthalpy of the gas entering or leaving the control volume. The term $\dot{m}\,(h_{\mathrm{ex}} - h)$ accounts for the energetic gain/loss due to intake/exhaust at the boundaries of the gas volume, that is estimated as:

$$\dot{m}\,(h_{\mathrm{ex}} - h) = \begin{cases} 0 & \text{if} \quad \dot{m} < 0 \\ \dot{m}c_{\mathrm{p}}\,(T_{\mathrm{ext}} - T_{\mathrm{l}}) & \text{if} \quad \dot{m} > 0 \end{cases} , \tag{6}$$

where T_{ext} is the external temperature in the crank case, assumed to be equal to the room temperature (290 K) and the bulk gas temperature is estimated by the line-averaged temperature T_{l}.

Figure 6 shows the heat flux density $\dot{q} = \dot{Q}\,/\,S_{\mathrm{w}}$ thus obtained together with the mean wall heat flux density calculated with the CFD code, as functions of the crank angle θ. A general agreement in terms of phase and magnitude is observed, with the greatest heat flux leaving the system just before TDC. During expansion, heat conduction from the wall to the gas results in a local heating of the boundary layer, i.e. a hotter gas in the boundary layer than in the bulk at BDC. Therefore, during the upstroke, the boundary layer gas is hotter than the bulk and the heat transfer is greater during compression, especially just before TDC because of the compressive heating, the locally hotter temperature and compression of the boundary layer thicknesses at piston and cylinder heads. The peak occurs before TDC because there is a relaxation of thermal profile while the piston is near the top of the stroke.

A non-dimensional cyclic lost work Ψ is defined according to Kornhauser and Smith [3]:

$$\Psi = \frac{\oint P\,\mathrm{d}V}{P_0 V_0 \left(\frac{P_{\mathrm{a}}}{P_0}\right)^2 \frac{\gamma-1}{\gamma}} \quad , \tag{7}$$

where P_0 is the cycle average pressure and P_{a} the mean-to-peak amplitude of pressure oscillation. For CFD, Ψ represents the heat transfer loss since it is the only loss mechanism. In the experiment however, Ψ represents the total loss. We thus define the non-dimensional thermal loss, Ψ_{th} as:

$$\Psi_{\mathrm{th}} = \frac{\int \dot{Q}\,\mathrm{d}t}{P_0 V_0 \left(\frac{P_{\mathrm{a}}}{P_0}\right)^2 \frac{\gamma-1}{\gamma}} \quad . \tag{8}$$

For a rotational speed of 109.34 RPM, the total non-dimensional cyclic loss is found to be:

for the CFD: $\Psi^{\mathrm{CFD}} = \Psi_{\mathrm{th}}^{\mathrm{CFD}} = 0.14$;
for the experiment: $\Psi^{\mathrm{XP}} = 0.32$ and $\Psi_{\mathrm{th}}^{\mathrm{XP}} = 0.25$.

The share of heat transfer in the experimental cyclic loss is predominant – $\Psi_{\mathrm{th}}^{\mathrm{XP}}$ represents 78% of the total experimental loss, Ψ^{XP}. Yet, it is largely underestimated by the CFD – $\Psi_{\mathrm{th}}^{\mathrm{CFD}}$ represents only 56% of $\Psi_{\mathrm{th}}^{\mathrm{XP}}$. This can be due to different causes. First, mass leakage might disturb the thermal boundary layers, thus resulting in a real heat transfer hardly described by CFD in an ideal gas spring. Second, the mass in the experimental system is estimated from a line-averaged temperature, while it should be calculated from the mass-averaged temperature, T_{m}.

Losses over a range of frequencies

The non-dimensional cyclic loss Ψ is calculated for a range of frequencies. The results are plotted in Figure 7 as a function of the oscillatory Péclet number Pe_ω, first introduced by Pfriem [1]:

$$\mathrm{Pe}_\omega = \frac{\omega {D_{\mathrm{h}}}^2}{4\alpha} \quad , \tag{9}$$

where ω is the rotational speed in rad/s, α is the gas thermal diffusivity at midstroke and D_{h} the hydraulic diameter at midstroke.

For high Péclet numbers ($Pe_\omega > 100$), a decrease of cyclic loss with increasing crankshaft rotational speed was also observed in Kornhauser and Smith's [3] experiments. As the frequency of the oscillating piston increases, the duration of a cycle

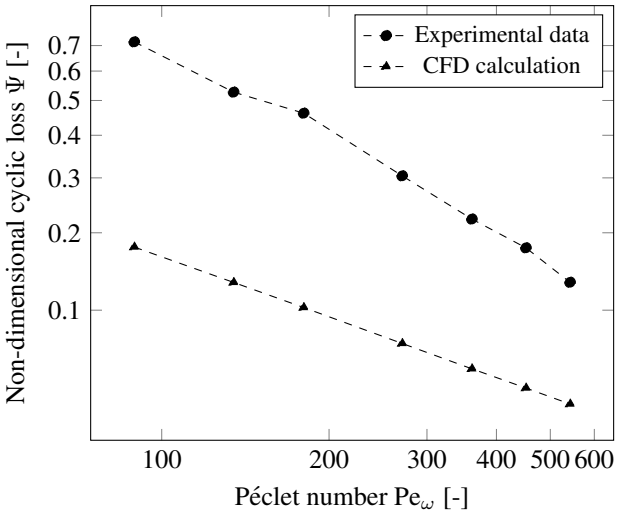

Figure 7. Non-dimensional cyclic loss Ψ over a range of Péclet numbers. For CFD, Ψ represents the heat transfer loss. For the experiment, the Ψ is the combination of heat and mass loss.

decreases. As a result, the loss mechanisms – either the heat exchange between the gas and the surrounding or the mass flux – have less time to significantly affect the gas system. The higher the Péclet number, the closer compression and expansion are to adiabatic processes.

CONCLUSION

In this article, experimental measurements on a crankshaft driven gas spring are compared to CFD simulations.

In the experimental setup, two loss mechanisms are in play. The unsteady heat transfer between the rapidly compressed-expanded gas and the surrounding walls and the mass leakage both adversely affect the thermodynamic performance of the device. To decouple these two loss mechanisms, three bulk parameters are measured. The volume is calculated from the crank angle recorded with a shaft encoder during the whole run. The pressure is measured with a pressure transducer connected to the top of the gas space. And the inner gas temperature is measured by an in-house developed system using ultrasonic transducers to determine the speed of sound in the gas.

A 2D-axisymmetric CFD model has been developed to predict heat transfer processes in an ideal gas spring, i.e. without mass leakage. Ideal gas law, mass, momentum and energy equations are solved within a dynamic mesh.

Experimental data are compared to the computed results for a single run at 109.34 RPM. Pressure-Volume and Temperature-Volume diagrams show a good general agreement, with the highest deviation observed at top dead center (TDC), where the mass leakage are expected to be the most important. By solving the energy balance for the experimental gas spring, the share of heat transfer in the total cyclic loss is calculated and found to be the major loss mechanism. Indeed, mass leakage accounts for only 22% of the total loss for the run at 109.34 RPM. While a general agreement in terms of phase and magnitude is observed between the measured and computed instantaneous heat fluxes, CFD calculation fails to predict the net loss due to heat transfer through one cycle (the numerical heat loss represents only 56% of the experimental thermal loss at 109.34 RPM). A physical explanation could be that the thermal boundary layers are disturbed by the mass flows due to the leakage in the clearance between the piston and the cylinder. Another source of error is that the mass flow in the experimental setup is calculated from a line-average temperature.

The next step is thus to establish, thanks to the temperature and density fields calculated in the CFD model, a relation between the line-averaged temperature obtained with the ultrasonic sensors and the bulk and mass-averaged gas temperatures, for a better estimation of both mass leakage and thermal loss in the experimental apparatus.

ACKNOWLEDGMENT

This work was supported by the UK Engineering and Physical Sciences Research Council (EPSRC) [grant number EP/J006041/1].

REFERENCES

[1] Pfriem, H., Periodic heat transfer at small pressure fluctuations, *NACA Technical Memorandum*, No. 1048, Sept. 1943.

[2] Lee K., A simplistic model of cyclic heat transfer phenomena in closed spaces, *Proceedings of the 18th Intersociety Energy Conversion Engineering Conference*, 1983, pp. 720-723.

[3] Kornhauser, A.A., and Smith, J.L., The effects of heat transfer on gas spring performance, *Journal of Energy Resources Technology*, Vol. 115, No. 1, 1993, pp. 70-75.

[4] Kornhauser, A.A., and Smith, J.L., Application of a complex Nusselt number to heat transfer during compression and expansion, *Journal of Heat Transfer*, Vol. 116, No. 3, 1994, pp. 536-542.

[5] Mathie R., White A.J., and Markides C.N., Ultrasonic measurements of unsteady heat transfer in a reciprocating gas spring, *Proceedings of the 10th International Conference on Heat Transfer, Fluid Mechanics and Thermodynamics*, 2014.

[6] Span, R., Lemmon, E.W., Jacobsen, R.T., Wagner, W., and Yokozeki, A., A reference equation of state for the thermodynamic properties of nitrogen for temperatures from 63.151 to 1000 K and pressures to 2200 MPa, *Journal of Physical and Chemical Reference Data*, Vol. 29, No. 6, 2000, pp. 1361-1433.

[7] Adair R.P., Qvale E.B., and Pearson J.T., Instantaneous heat transfer to the cylinder wall in reciprocating compressors , *Proceedings of the 1st International Compressor Engineering Conference*, Paper 86, 1972.

[8] Lekić, U., and Kok, J.B.W., Heat transfer and fluid flows in gas springs, *Open Thermodynamics Journal*, Vol. 4, 2010, pp. 13-26.

[9] Taleb A., Sapin P., Barfuss C., White A.J., Fabris D., and Markides, C.N., Wall temperature and system mass effects in a reciprocating gas spring, *Proceedings of the 29th International Conference on Efficiency, Cost, Optimisation, Simulation and Environmental Impact of Energy Systems (ECOS)*, 2016.